Chapter 4

DOES BULK RELATIVISTIC MOTION OCCUR ON A LARGE SCALE ?

Do the relativistic speeds inferred in the nuclei of radio quasars persist out to the large scale jets and hot spots that are several hundred kiloparsecs away? Kapahi (1981a) examined the conjecture that extragalactic radio sources of suspected one-sided structure were actually those with large apparent side-to-side asymmetry that arose out of relativistic Doppler effects. The data that he compiled for all such objects known at the time supported this conjecture. These sources would *then* be oriented close to the line of sight, and at least mild bulk relativistic motion would be implied not only in the jets but also in the hot spots.

The availability of better quality data for the sample of Kapahi (1981a) enable a more stringent test of this hypothesis, and this is the focus of the present chapter. Radio images of high angular resolution presented in Chapter 3 form the main body of data used; a systematic examination of the behaviour of asymmetry in radio morphology in the context of the relativistic beaming hypothesis has been attempted therefrom. The basic idea of the unified scheme, viz., that the prominence of the nuclear radio component (R) is a statistical measure of the angle of inclination to the line of sight (e.g., Kapahi & Saikia, 1982) is used. While there is good evidence for the occurrence of bulk relativistic motion in radio quasars, the case for radio galaxies and radio-quiet quasars is not as clear. Especially in radio galaxies that are of Fanaroff-Riley type I (Fanaroff & Riley, 1974), it is very likely that the bulk velocities of the radio-emitting effluents are subrelativistic. The analysis is therefore

restricted to radio-loud quasars.

The sample of the Kapahi (1981a) is slightly reconstituted in view of the data presented in chapter 3, and properties that are expected to be a function of the orientation with respect to the line of sight are derived. These properties are then compared with those of three quasar samples selected to be both more and less extreme in their orientation with respect to the line of sight (as per the relativistic beaming scenario).

4.1 The new sample

The sample of radio sources selected for study of asymmetry in radio structure was mostly drawn from the list of Kapahi (1981a). Various facts, mostly revealed by high resolution images of these objects (either from Chapter 3 or from the literature) warrant exclusion of some sources from the analysis that follows. All additions to and deletions from the sample of Kapahi (1981a) are described below. The sample thus reconstituted shall be referred to hereinafter as the **D2 sample** (so named after the nomenclature of Miley, 1971).

The following objects, not in Kapahi (1981a), were included in the D2 sample (cf. chapter 2): 0232-042, which was tentatively classified as one-sided by Miley & Hartsuijker (1978); 0717+170, which was suspected to have one-sided structure by Joshi (1981); 1007+417, which was found one-sided by Kapahi (1981b) but two-sided by Miley & Hartsuijker (1978); 2325+269, which was found to be one-sided by Miley & Hartsuijker (1978) and two-sided by Potash & Wardle (1979). VLA images for all of these objects have been presented in chapter 3.

Objects in the list of Kapahi (1981a) whose optical identification is in doubt are not included in the D2 sample. These are: 0615+578, the original identifications for which were later found to be stars; 0717+170, 0814+201 and 2041-149, in the case of all of which the new VLA images call into question the identifications previously suggested (cf. section 3.3).

In the cases of 0740+380, 1047+096, 1320+299 and 1419+315, what had been previously regarded as the "central component" (associated with a QSO) has been revealed to be almost certainly an independent quasar. The "outer component" is in each case almost certainly a physically distinct object, juxtaposed by chance near the identified quasar. They have therefore not been included in the D2 sample.

What was regarded as the "core component" of 1203+109 and 2251+134 turns out to be an independent triple source. The "outer component" of the earlier observations remains undetected. These objects have been excluded.

All radio galaxies and radio-quiet quasars have been excluded from the D2 sample because the focus of this study is the evidence for relativistic bulk motion in radio-loud quasars. Therefore, only radio-loud quasars are included in the D2 sample. Hence, the following objects were eliminated:

* 0241+622, which actually belongs to the class of radio-quiet QSOs. It is of relatively low radio luminosity, and is detectable easily at radio wavelengths only due to its proximity to us. Also, it probably inhabits a spiral galaxy (cf. description in section 3.3), while radio loud quasars are known to usually reside in elliptical galaxies.

* 0309+411, 1350+316 and 1807+698, each of which is optically identified with an elliptical galaxy.

The 36 objects in the D2 sample are listed in **Table 4.1.**

4.2 The comparison samples

Three samples of quasars have been chosen for comparison of properties with the D2 sample. The first two are expected to have most of their objects inclined at relatively small angles to the plane of the sky, while the third is expected to consist of quasars inclined extremely close to the line of sight. The three comparison samples are described below. Their constituent objects are listed in **Tables 4.2 to 4.4** respectively.

4.2.1 The 3CR sample

This is the extremely well-known and extensively studied sample of extragalactic radio sources derived from the the 3rd Cambridge Radio survey at 178 MHz (Laing *et al.*, 1983). The sample has a flux density limit of 10 Jy at this frequency. The low survey frequency has resulted in the selection of objects that are mostly of the steep radio spectrum type, since those of flat radio spectrum are rarely bright enough at this frequency. It is expected in the unified scheme that quasars from this sample would be oriented randomly in the sky.

There are 44 quasars in the 3CR sample. Redshifts are available for all the objects. Radio images obtained with the VLA are available in the literature for most of them, and these data were used to derive their properties that are of interest here. In exceptional cases it was necessary to use lower resolution images obtained with

Table 4.1 The D2 sample of quasars: derived properties.

Source	Alternate Name	z	R	Linear Size kpc)	Surface Brightness Ratio	Separation Ratio
0115+027	4C02.04	0.672	0.32	105	1.3	1.4
0232-042	4C-04.06	1.436	0.23	113	2.8	3.3
0409+229	4C22.08	1.215	1.30	39	5.5	0.9
0742+376	4C37.19		0.40	530	> 32.5	
0821+394	4C39.23	1.216	13.85	40	> 1.7	
0836+195	4C19.31	1.691	0.47	263	22.7	0.8
0836+710	4C71.07	2.160	16.52	16	> 12.0	
0919+218	4C21.25	1.421	0.07	96	27.0	1.3
0932+022	4C02.27	0.659	0.31	370	4.0	0.2
0945+408	4C40.24	1.252	2.15	35	> 4.0	
1007+417	4C41.21	0.611	0.27	245	14.4	1.7
1012+232	4C23.24	0.565	7.53	134	4.1	2.0
1040+123	3C245	1.029	3.01	63	18.6	1.7
1055+018	4C01.28	0.888	35.75	251	2.0	
1055+201	4C20.24	1.110	2.26	182	> 54.8	
1132+303	4C30.22	0.614	0.27	119	5.1	1.2
1136-135	PKS	0.554	0.28	118	5.9	1.7
1203+109	4C10.34	1.088	0.48	48	2.8	0.8
1222+216	4C21.35	0.435	1.58	112	6.1	1.2
1226+023	3C273	0.158	3.57	75	>500.0	
1347+539	4C53.28	0.976	4.04	45	> 3.0	
1354+195	4C19.44	0.720	4.85	351	1.2	1.8
1415+463	4C46.29	1.552	4.45	112	> 27.4	
1433+177	4C17.59	1.203	0.46	86	8.4	0.9
1509+158	4C15.45	0.828	0.16	69	12.4	4.0
1636+473	4C47.44	0.740	3.35	162	> 20.0	
1637+574	OS 562	0.745	36.49	32	> 1.8	
1641+399	3C345	0.595	29.78	22	> 13.0	
1642+690	4C69.21	0.751	9.33	81	> 34.0	0.7
1729+501	4C50.43	1.107	0.07	175	>117.3	
1741+279	4C27.38	0.372	0.59	63	5.7	1.3
1800+440	OU401	0.660	1.83	80	1.2	0.3
1842+681	JB	0.475	26.16	28	> 3.0	
2037+511	3C418	1.687	4.76	25	> 50.0	
2251+158	3C454.3	0.859	35.00	44	> 5.5	
2325+269	4C27.52	0.875	0.10	62	9.0	1.1

the Cambridge interferometer (Laing, 1981; Jenkins *et al.*, 1977).

4.2.2 The SSH sample

Swarup *et al.* (1984) published radio images of 31 radio-loud quasars obtained with the VLA. The quasars were selected from among those that lie close to the upper envelope of the largest-angular-size vs. redshift diagram. Thus, foreshortening due to projection would not be significant for these quasars, and they would be expected to lie close to the plane of the sky.

Swarup *et al.* (1984) remark that the radio structure of 0911+053 is uncertain, because there is lack of consistency among different data available for the object. Also, their data show that in the case of 2318+026, the association of the QSO with the central radio component is uncertain. The sample constituted after excluding these two objects thus contains 29 quasars, and is designated as the **SSH sample.**

4.2.3 The OBC sample

O'dea *et al.* (1986; 1988) have presented radio images of 16 quasars obtained with the VLA. The quasars were selected to be strongly core-dominant. In the unified scheme, these radio sources would have their radio axes oriented close to the line of sight. This sample, designated the **OBC sample**, was thus chosen to represent the opposite extreme in radio axis orientation vis-a-vis the 3CR and SSH samples.

4.3 Compact Steep Spectrum Quasars

It has recently become clear that while extragalactic sources that have flat radio

Table 4.2 The 3CR sample of quasars: derived properties.

Source	Alternate Name	z	R	Linear Size kpc)	Surface Brightness Ratio	Separation Ratio
0017+154	3C9	2.012	< 0.002	95	4.0	1.0
0033+183	3C14	1.469	0.01	198	1.3	0.5
0133+207	3C47	0.425	0.07	450	8.0	1.2
0229+341	3C68.1	1.238	<0.0003	482	48.0	0.6
0710+118	3C175	0.768	0.06	396	1.6	0.8
0758+143	3C190	1.195	0.10	58	1.3	1.7
0833+654	3C204	1.112	0.06	301	1.1	1.4
0835+580	3C205	1.534	0.02	145	1.4	1.2
0838+133	3C207	0.684	0.69	100	2.7	1.2
0850+140	3C208	1.110	0.05	110	6.3	1.1
0855+143	3C212	1.048	0.15	84	3.3	0.9
0903+169	3C215	0.411	0.06	199	2.5	0.5
0906+430	3C216	0.670	1.34	24	6.3	0.8
1040+123	3C245	1.029	3.01	63	18.6	1.7
1100+772	3C249.1	0.311	0.13	130	2.4	0.5
1111+408	3C254	0.734	0.02	107	1.2	0.1
1137+660	3C263	0.646	0.14	336	33.3	0.6
1206+439	3C268.4	1.400	0.04	88	3.8	0.9
1218+339	3C270.1	1.519	0.18	79	3.6	0.8
1241+166	3C275.1	0.557	0.14	131	1.4	1.5
1258+404	3C280.1	1.659	0.07	196	6.7	1.5
1549+628	3C325	0.860	< 0.08	145	1.6	0.5
1618+177	3C334	0.555	0.42	338	1.3	0.6
1622+238	3C336	0.927	0.03	192	1.2	2.1
1641+399	3C345	0.595	29.78	22	>13.0	
1704+608	3C351	0.371	0.01	365	2.4	0.8
1732+160	4C16.49	1.880	0.02	128	1.2	1.7
2120+168	3C432	1.805	0.01	112	1.1	0.6
2251+158	3C454.3	0.859	35.00	44	>5.5	

Table 4.3 The SSH sample of quasars: derived properties.

Source	Alternate Name	z	R	Linear Size kpc)	Surface Brightness Ratio	Separa-tion Ratio
0118+034	3C39	0.765	0.12	360	2.0	1.0
0133+207	3C47	0.425	0.07	450	8.0	1.2
0229+341	3C68.1	1.238	<0.0003	482	48.0	0.6
0312-034	4C-3.11	1.072	0.01	361	1.8	1.1
0808+289	B2	1.910	1.55	496	4.0	1.7
0835+580	3C205	1.534	0.02	145	1.4	1.2
0901+285	B2	1.121	0.53	202	3.3	1.1
0903+169	3C215	0.411	0.06	199	2.5	0.5
0922+149	4C14.31	0.896	0.11	345	3.0	1.2
0932+022	4C02.27	0.659	0.31	370	4.0	0.2
0957+003	4C00.34	0.907	0.23	282	2.4	1.3
1004+130	4C13.41	0.240	0.04	551	2.9	1.5
1011+280	4C28.25	0.899	0.63	122	2.5	0.7
1100+772	3C249.1	0.311	0.13	130	2.4	0.5
1137+660	3C263	0.646	0.14	336	33.3	0.6
1221+186	4C18.34	1.401	0.24	203	1.1	1.4
1244+324	4C32.41	0.949	0.29	207	1.7	0.9
1248+305	4C30.25	1.061	0.02	243	4.2	1.2
1305+069	3C281	0.599	0.04	312	9.5	0.7
1435+315	B2	1.366	2.48	103	1.6	0.5
1545+210	3C323.1	0.264	0.07	358	1.8	0.7
1602-001	4C-0.63	1.625	0.43	225	1.8	2.4
1606+289	4C28.40	1.689	0.04	251	1.9	0.9
1618+177	3C334	0.555	0.42	338	1.3	0.6
1622+238	3C336	0.927	0.03	192	1.2	2.1
1704+608	3C351	0.371	0.01	365	2.4	0.8
1739+184	4C18.51	0.186	0.15	850	2.0	1.0
2131+175	4C17.87	1.215	0.16	267	1.8	1.0
2325+293	4C29.68	1.015	0.06	426	22.8	0.9

Table 4.4 The OBC sample of quasars: derived properties.

Source	Alternate Name	z	R	Linear Size kpc)	Surface Brightness Ratio	Separation Ratio
0224+671			13.07	255	7.5	
0333+321	NRAO140	1.263	50.19	69	3.1	1.8
0605-085		0.870	22.01	46	> 7.0	
0735+178			37.24	17	> 2.0	
0836+710		2.160	16.52	16	> 12.0	
0859-140		1.327	49.05	103	> 2.5	
1055+018	4C01.28	0.888	35.75	251	2.0	
1116+128		2.118	5.97	24	> 50.0	
1510-089		0.361	15.52	55	> 4.0	
1624+416			32.65	9	> 16.0	
1633+382		1.814	162.04	100	> 1.2	
1642+690	4C69.21	0.751	9.33	81	> 34.0	0.7
1749+701			123.46	3	> 2.5	
1807+698	3C371	0.051	56.78	394	> 25.0	
1823+568		0.664	7.27	118	> 66.7	
2037+511	3C418	1.687	4.76	25	> 50.0	

Table 4.5 Compact Steep Spectrum quasars in the 3CR sample.

Source	Alternate Name	z	R	Linear Size (kpc)
0127+233	3C43	1.459	4.75	21
0134+329	3C48	0.367		8
0518+165	3C138	0.759		5
0538+498	3C147	0.545	3.38	10
0725+147	3C181	1.382	0.01	50
0740+380	3C186	1.063	0.03	14
0802+103	3C191	1.956	0.04	40
0809+483	3C196	0.871	0.00	48
1328+254	3C287	1.055		1
1328+307	3C286	0.849	3.83	22
1458+718	3C309.1	0.905	1.46	18
1634+628	3C343	0.988	58.75	9
1828+487	3C380	0.692	0.57	7
2249+185	3C454	1.757		5
2252+129	3C455	0.543	0.12	24

spectrum over a large frequency range are almost invariably of small projected linear sizes, those with steep radio spectrum, while usually large, *are sometimes also of small linear dimensions* (Kapahi, 1981b; Peacock & Wall, 1982; van Breugel *et al.*, 1984a). These latter have been termed Compact Steep Spectrum (CSS) sources, and they include both radio galaxies and radio-loud quasars. Van Breugel *et al.*, 1984a argued that the combination of compactness and steepness of spectrum in the CSS objects was due to strong interaction of the radio emitting effluents with the (gas rich) interstellar medium. Thus, they are almost certainly a class of objects that is physically distinct from the CDQs and the LDQs. If the interactions with the surrounding medium are indeed significant, they could well intensify the intrinsic radiative dissipation from the radio emitting material, instead of (or in addition to!) relativistic bulk motion enhancing the apparent emission.

More recent VLBI studies have shown that the nuclear radio structures in CSS quasars are often complex (Fanti *et al.*, 1988; Nan *et al.*, 1988), suggestive of interaction of the twin-beams with the interstellar medium. If so, the prominent nuclear radio components sometimes seen in CSS quasars could be a reflection of this interaction, in which case *R would no longer be a statistical measure of the angle of inclination of the radio axis to the line of sight.* It may be noted that the CSS quasars could then fortuitously contribute to the correlation of R with projected linear size (l), and also to the correlation of R with misalignment of radio structure (since the strong interaction with the interstellar medium is likely to produce relatively large intrinsic bends in the jets). It is therefore not appropriate to include

the CSS quasars in analyses that test the unified scheme for samples of quasars.

The following operational definition of a CSS quasar has been adopted hereinafter. A radio quasar that has most of its radio flux density in a component of steep radio spectrum (i.e., $\alpha < -0.5$) in the radio frequency range between 1 and 15 GHz, and has a projected linear size < 50 kpc is regarded as a CSS quasar. The cutoff values chosen for α and l are necessarily somewhat arbitrary, but the intention is to include objects of steep radio spectrum over a reasonably wide frequency range, and of subgalactic linear dimension. It may be noted that deep and high resolution imaging at optical wavelengths have revealed that the host galaxies of radio-loud quasars have sizes of about 40 to 80 kpc for H_0 of 50 km s^{-1} Mpc^{-1} and q_0 of 0.5 (e.g., Hutchings, 1987: 25 to 60 kpc for H_0 of 100 km s^{-1} Mpc^{-1} and q_0 of 0).

In the case of the D2 sample, 0003-003, 0051+291 (both described in Chapter 3) and 1828+487 (Pearson *et al.*, 1985) qualify as CSS quasars under the above definition and have been excluded from the analysis. In the case of the 3CR sample, 15 quasars are CSS objects (Table 4.5); they have been excluded. Note that of the 11 for which the image resolutions are sufficient to delineate the core and determine R, six have R > 0.5. Neither the SSH nor the OBC sample contain any CSS quasars.

4.4 The derived properties of quasars

To do the comparative analysis of the four samples of quasars, the prominence of the nuclear radio component R_{emit}, the projected linear size l, the ratio of surface

brightness of the peaks of the outer components, and the ratio of the angular separation of these peaks from the nuclear component have been evaluated for each quasar. The definitions of these parameters and the methods by which they are calculated are given below. The parameter values for the four samples are listed in Tables 4.1 to 4.4.

4.4.1 The prominence of the nuclear component

The prominence of the nuclear radio component R_{emit}, is defined as the ratio of the radio emission from the nuclear component to that from the extended structure, evaluated at an emitted frequency of 8 GHz (in the rest frame of the quasar). It is more accurate to use the frequency of emission in the rest frame rather than the observed frequency of emission because the nuclear and outer components usually have very different spectral indices. The emitted frequency was chosen to be 8 GHz to minimize errors due to the fact that the exact spectral indices of the components are unknown (most of the flux densities are measured near 5 GHz).

The radio spectral indices of the components actually need to be derived from multi-frequency images of comparable resolution, which are unavailable in most of the cases. Therefore, it has been assumed here that the nuclear components have a spectral index of 0 and the extended outer components have a spectral index of -1. The former is the median value of spectral indices for the quasars observed by Perley (1982) between wave bands of $\lambda 6$ and 20cm. The latter is the median value of spectral indices for the extended components of the 3CR quasars (Laing & Peacock, 1980). Thus,

$$R_{emit} = \left[\frac{S^{nuc}}{\left(S^{tot} - S^{nuc}\right)}\right]\left[\frac{8.0}{\nu^{tot}(1+z)}\right],$$

where S^{nuc} and S^{tot} are the nuclear and total radio flux densities respectively, and ν^{tot} is the observing frequency at which the total flux density was measured.

The flux densities of the nuclear components have been measured in the $\lambda 6$ cm band in all cases, except 0232−042 (where it is measured at 15 GHz) and 1222+216 (where it is measured at 1.4 GHz). Both these objects belong to the D2 sample. Most of the total flux densities have been measured at $\lambda 6$ cm too, unless unavailable, in which case values at $\lambda 11$ or 18 cm, have been used. Single-dish measurements have been used for the total flux density except where unavailable, in which case interferometric measurements are used. The derived values of R_{emit} for the quasars in the four samples are listed in column 4 of the Tables 4.1 to 4.4.

4.4.2 The projected linear size

The projected linear size l of each of the quasars is given by

$$l = \left\{(LAS)\frac{c}{[H_0 q_0^2 (1+z)^2]}\right\}\left\{zq_0 + (q_0-1)[-1 + (2q_0 z + 1)^{1/2}]\right\}$$

where LAS, the largest angular size, is the angular separation between the outermost surface brightness peaks of radio emission of the quasar. H_0 is assumed to be 50 km s^{-1} Mpc^{-1} and q_0 to be 0.5. The calculated values of l are listed in column 5 of Tables 4.1 to 4.4.

4.4.3 The surface brightness ratio of the outer components

The ratio of the radio surface brightness of the peaks of the outer components on either side of the core component (estimated with the value of the brighter peak in the numerator by convention) is taken to be a measure of the asymmetry in side-to-side emission. This parameter will hereinafter be referred to as the surface brightness ratio. In the case of the D2 sample, the estimates have mostly been made using the VLA data presented in Chapter 3. In all other cases, data from the literature have been used, and if the values of the surface brightness of the peaks are not themselves listed, they have been estimated from the published radio images. In most of these cases, the data are from the VLA. Data from the Cambridge interferometer were used for the exceptions, which are 0710+118, 1549+628 (both from Jenkins *et al.*, 1977) and 0833+654 (Laing, 1981). (All three objects are from the 3CR sample.)

The surface brightness ratio has been evaluated at λ6 cm wavelength, and if unavailable, then at λ11 or 20 cm. In cases where an outer lobe has been detected on only one side of the nuclear component, a lower limit to the surface brightness ratio has been evaluated, using three times the quoted r.m.s. value of the image, or the lowest/second lowest contour of surface brightness plotted. The values of this parameter are listed in column 6 of Tables 4.1 to 4.4.

4.4.4 The separation ratio of the outer components

The ratio of the angular separation of the brightest peak of the extended radio emission to the separation of the brightest peak on the opposite side of the core

component (hereinafter referred to as the "separation ratio") has been adopted as a measure of the asymmetry of projected separation of the outer components. Thus, for equidistant outer components the value is unity; if the component with a higher peak surface brightness is closer to the core, the value is, by convention, taken to be less than unity and vice versa. The values for each individual quasar are listed in column 7 of Tables 4.1 to 4.4.

4.5 The results—general consistency with the unified scheme

As was mentioned in section 4.2, the 3CR and SSH comparison samples were chosen to provide sets of quasars expected to be generally oriented closer to the plane of the sky than the D2 sample, and the OBC comparison sample is expected to be a set of quasars inclined close to the line of sight, perhaps even closer than the D2 sample. The results of the analysis are presented and discussed in this section.

4.5.1 The behaviour of surface brightness ratio and R

Fig 4.1a to d show the distribution of surface brightness ratio for the quasars in the 3CR, SSH, D2 and OBC samples respectively. (It may be noted that in the case of the OBC quasars, most of the values are lower limits because only one outer component has been detected.) The distributions for the D2 and OBC quasars show evidence for a large number of objects with very asymmetric surface brightness ratio. On the other hand, the distributions for the 3CR and SSH quasars peak at a much lower value and contain far fewer objects of large asymmetry. The distribution for the SSH quasars peaks at a marginally higher value than the 3CR quasars.

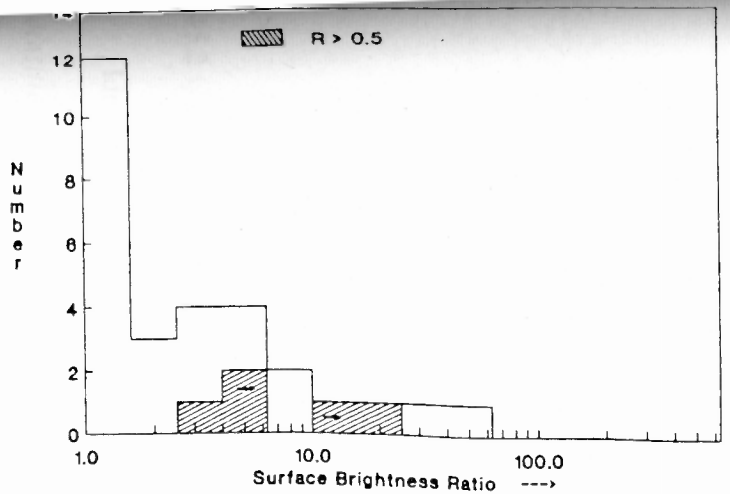

Fig.4.1a Distribution of surface brightness ratio for 3CR quasars

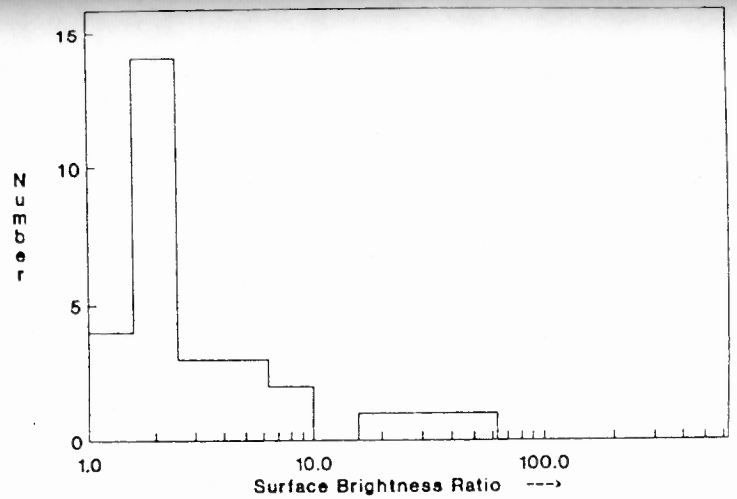

Fig.4.1b Distribution of surface brightness ratio for SSH quasars

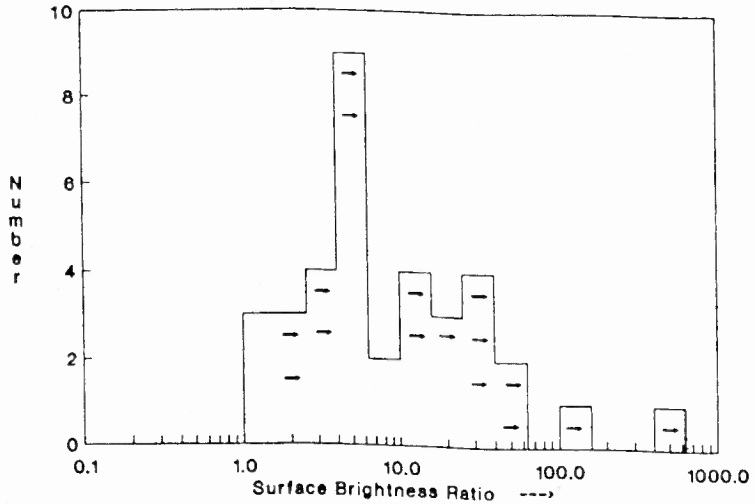

Fig.4.1c Distribution of surface brightness ratio for D2 quasars

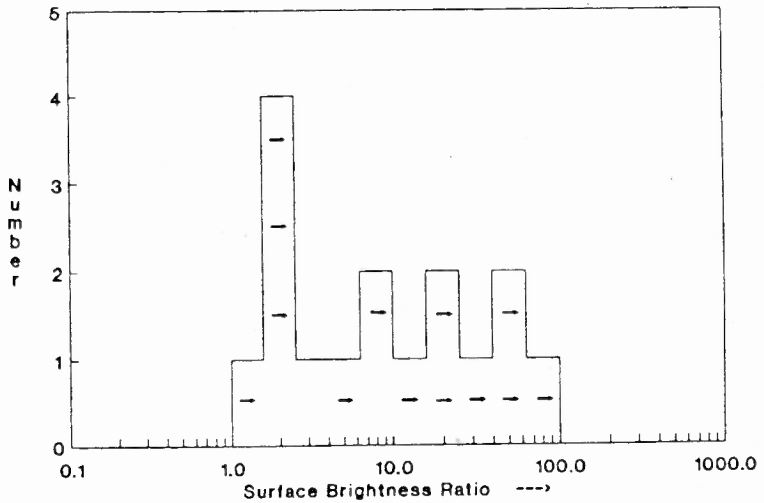

Fig.4.1d Distribution of surface brightness ratio for OBC quasars

Is the asymmetry related to the orientation inferred from the value of R? The distribution of R_{emit} for each of the samples is shown in Figs. 4.2a to d. The peak and median values of the distributions shift to larger values of R_{emit} as one moves from Fig.4.2a through to d, which parallels the trend in the distributions of surface brightness ratio. The median values of the distributions of R_{emit} and the surface brightness ratio for the four samples are given in Table 4.6. It is worth pointing out that there are a few objects in the 3CR sample with $R_{emit} > 0.5$. These have been marked hatched in the distribution of surface brightness ratio, and it turns out that four out of five of the objects are of surface brightness ratio > 4. *Thus the results are broadly consistent with the supposition that the hot spots at least mildly relativistic*, so that Doppler beaming plays a significant role in determining the side-to-side asymmetry.

Table 4.6 Median values of the distributions.

Sample of Quasars	R_{emit}	Projected Linear Size (kpc)	Surface Brightness Ratio	Separation Ratio
3CR	0.07	130	2.5	0.8
SSH	0.12	312	2.4	1.0
D2	2.0	84	6.0	0.5
OBC	27	62	7.3	-

4.5.2 Caveats

Ideally, to test if the outer hot spots are relativistically beamed, the *flux densities* of the hot spots need to be determined. For this, sufficient angular resolutions are required that will delineate what might be identified as the physical

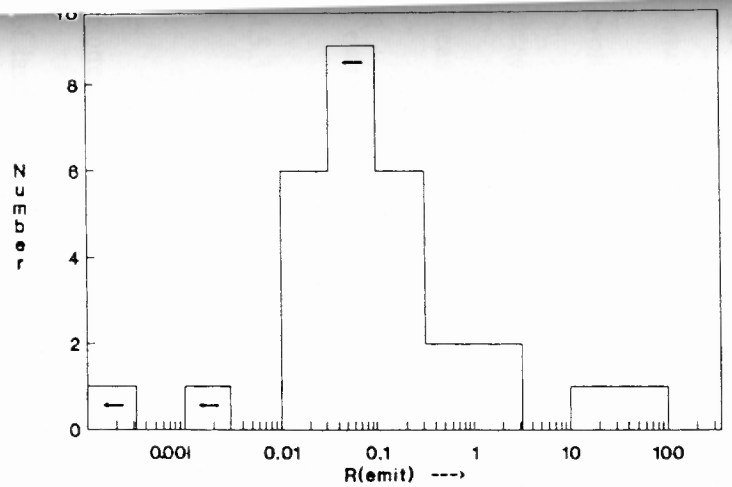

Fig.4.2a Distribution of R_{emit} for 3CR quasars

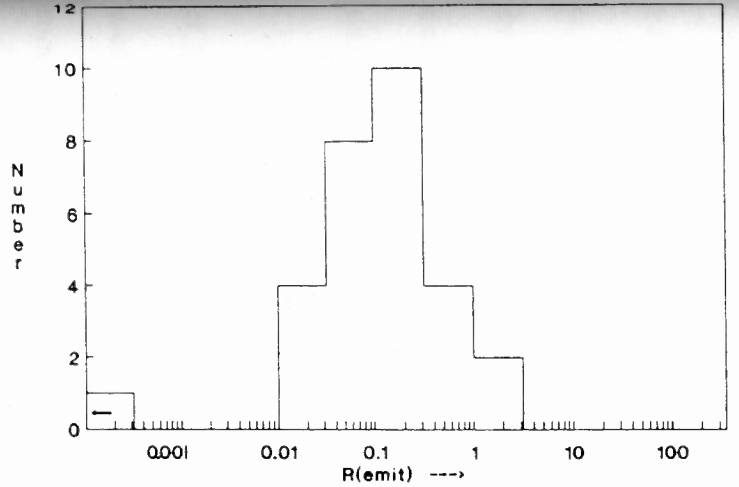

Fig.4.2b Distribution of R_{emit} for SSH quasars

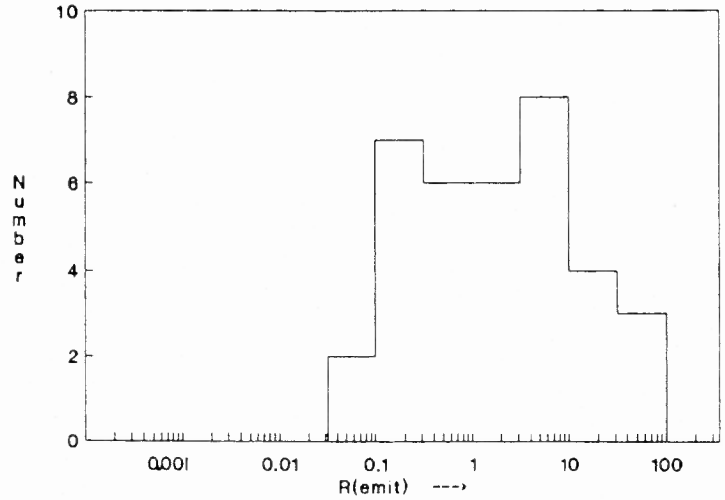

Fig.4.2c Distribution of R_{emit} for D2 quasars

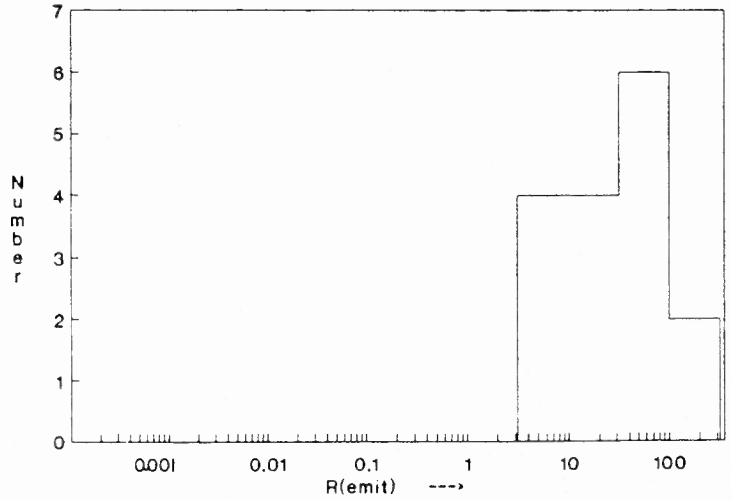

Fig.4.2d Distribution of R_{emit} for OBC quasars

hot spot, which is important because the surrounding (more diffuse) emission (from material which has emerged from the hot spot—e.g., Begelman *et al.*, 1984) is not expected to be relativistically beamed. But since the angular resolutions obtained for the body of data analyzed here are insufficient to determine these flux densities, the surface brightness ratio has been adopted as the next best measure of the side-to-side asymmetry in intensity.

The uncertainties in an analysis of this sort should be kept in mind. The value of the surface brightness ratio inferred would depend on the restoring beam-width used in the image. (Ideally, beam widths that are uniform for all the objects when converted to the linear scale should be used.) Further, even if flux densities of the hot spots *were* used, there is another complication. The two hot spots on the opposite sides are observed at different ages because of the light-travel-time between them, and therefore differences in hot-spot characteristics due their time-evolution could contribute to the observed asymmetry. It is interesting that despite these complications that could potentially mask any systematic effects, the adopted measure of the surface brightness asymmetry appears to show a gradation with R_{emit}.

4.5.3 The distribution of *l*

The distributions of projected linear size for the four samples respectively are plotted in Figs. 4.3a to d. The quasars in the SSH sample, which consists of objects of large angular size, have the largest projected linear sizes; those from the OBC sample have the smallest. The median values of these distributions are also listed in Table 4.6. The qualitative trend is roughly consistent with what was found by

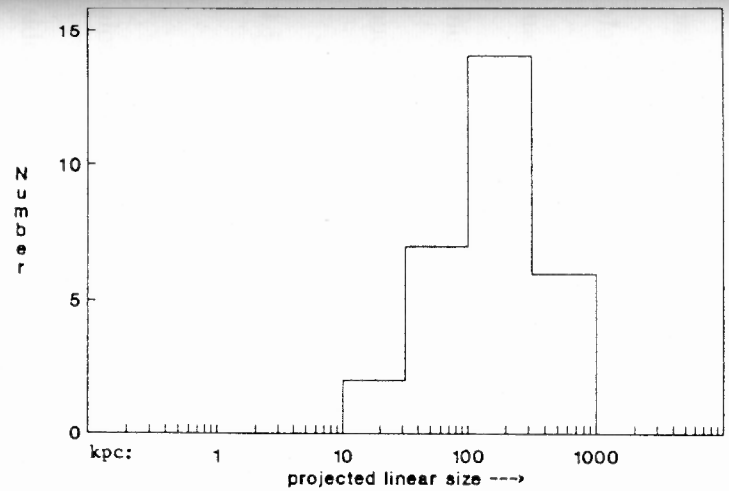

Fig.4.3a Distribution of projected linear size: 3CR quasars

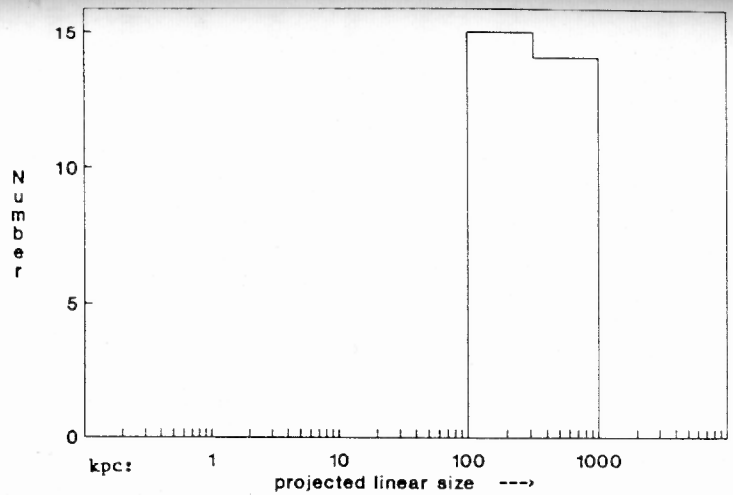

Fig.4.3b Distribution of projected linear size: SSH quasars

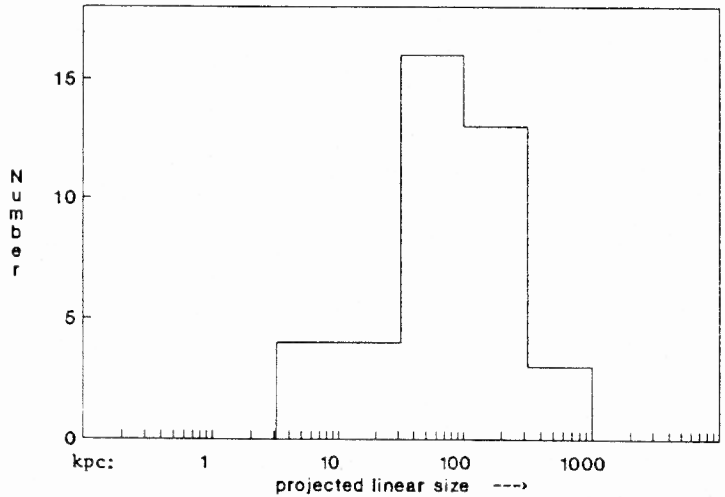

Fig.4.3c Distribution of projected linear size: D2 quasars

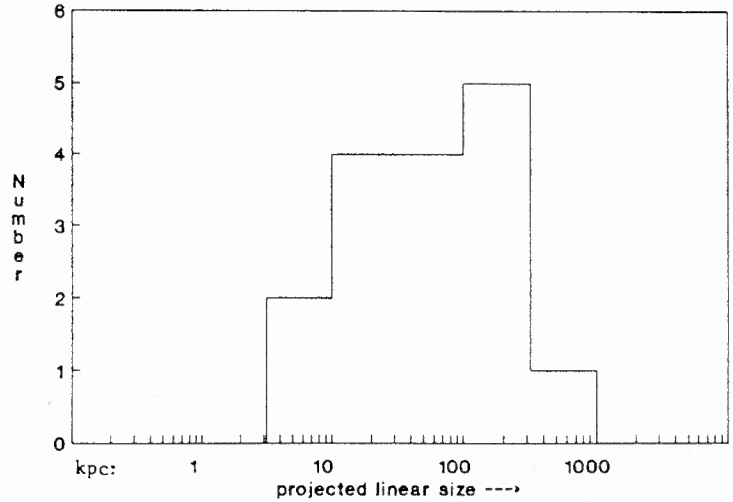

Fig.4.3d Distribution of projected linear size: OBC quasars

Kapahi & Saikia (1982), viz., that *the prominence of the nuclear component is inversely correlated with the projected linear size.*

Note that the 3CR quasars are expected to be randomly oriented in the sky. The quasars in the SSH sample, on the other hand, have been chosen to have the largest sizes, as indeed Fig. 4.3b shows. It is therefore expected that they are the least foreshortened objects, or, the ones closest to the plane of the sky. But this is not borne out by the R distributions; that for the SSH sample has higher values of peak and median than the 3CR distribution. Two possible factors could contribute to this apparent inconsistency. Firstly, the intrinsic linear size could be correlated with the Lorentz factor for the nuclear jets (e.g., Browne, 1987), in which case the largest quasars would have more prominent nuclear components. Secondly, the SSH quasars had to necessarily have a measured redshift, and redshifts are usually preferentially measured for the optically brighter objects. And if, as has been elaborated upon in Chapter 6, the Doppler boosting of the radio emission from the nuclear component is accompanied by enhancement of the optical continuum, there might well be a slight bias in the SSH sample of quasars towards objects with their nuclear jets inclined not so closely to the plane of the sky.

4.5.4 The separation ratio

The distributions of separation ratio for the 3CR, SSH and D2 samples are plotted in Figs. 4.4a to c. In the case of the OBC sample, outer components on both sides of the core component have been detected for only two objects, and therefore no distribution has been plotted. The D2 quasars show a marginally broader distribution than the other two samples, i.e., relatively larger deviations from unity

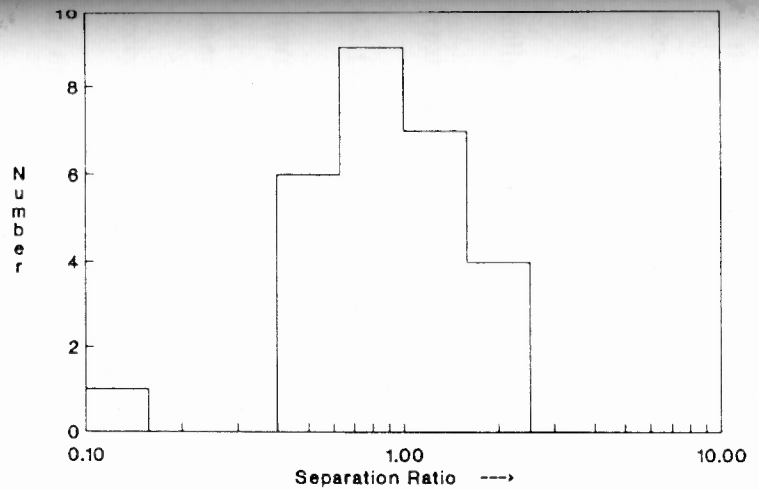

Fig.4.4a Distribution of separation ratio for 3CR quasars

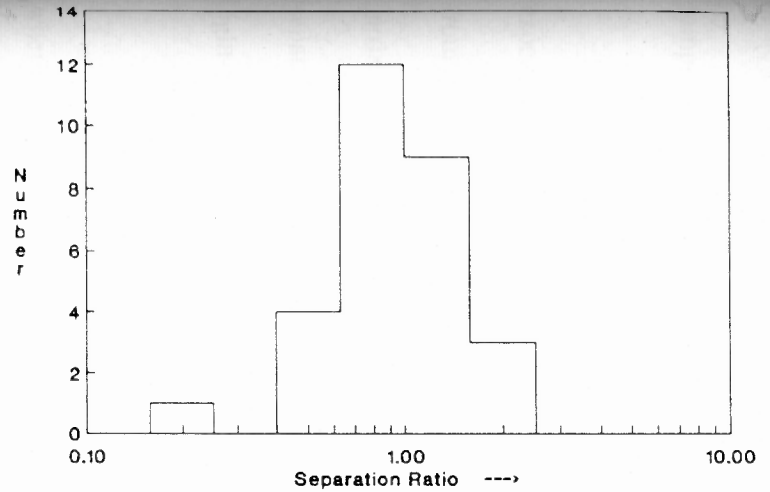

Fig.4.4b Distribution of separation ratio for SSH quasars

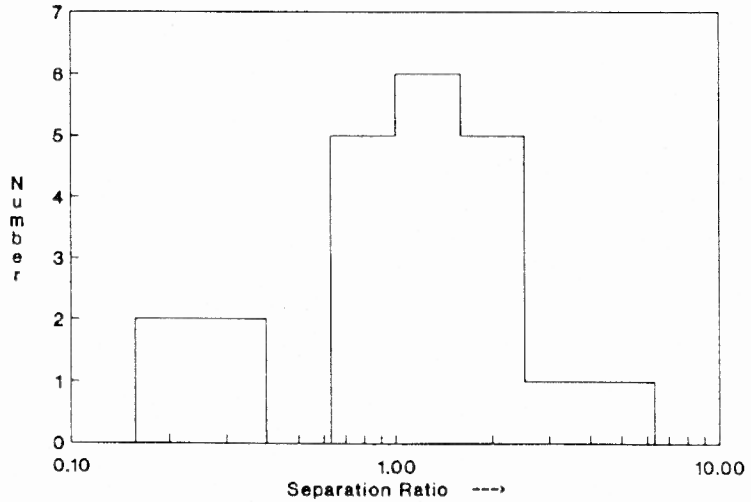

Fig.4.4c Distribution of separation ratio for D2 quasars

in both directions. The median values do not differ significantly across the three samples (see Table 4.6).

If the D2 quasars are relativistically beamed, then there are two reasons to expect the apparent separation ratio of an intrinsically symmetric quasar to differ from the value of unity. Firstly, the approaching outer component of a straight, intrinsically symmetric source would be observed at a later time and hence larger separation from the nucleus as compared to the receding outer component, due the light-travel-time difference. The observed separation ratio is thus given by

$$\frac{(1 + \beta\cos\theta)}{(1 - \beta\cos\theta)},$$

where βc is the velocity of advancement of the peaks of emission, and θ is the angle of inclination of the direction of motion to the line of sight. If the asymmetry in the surface brightness ratio is a consequence of differential Doppler beaming, then the brighter component is the approaching one, and the separation ratio would be greater than unity. Since the separation ratio increases with decrease in inclination angle θ, quasars inclined close to the line of sight would show large separation ratios (Kapahi & Saikia, 1982). Separation ratios of $\sim$ 1.4 obtain for β of 0.2 (and $\sim$ 2.5 for β of $\sim$ 0.5). Secondly, if any non-collinear ejection bends the approaching radio jet towards the line of sight, the separation ratio observed otherwise would be reduced, since the projected angular separation would then decrease relative to that of the receding component (Saikia, 1984a). Clearly, the two are opposing effects.

Further, whether or not relativistic beaming occurs, light-travel-time differences may be masked by differences in the characteristics of the interstellar/intergalactic

medium on either side of the nucleus. Differences in the surrounding media on either side could cause separation ratios to differ from unity.

4.5.5 Jet detectability accompanied by hot spot enhancement

Among the 20 quasars of the D2 sample for which two-sided emission has been detected, in 17 certain cases and 2 likely cases, the jet points towards the brighter of the two outer components. The exception to this trend is 0932+022. If the detectably high surface brightness of the jets were not due Doppler enhancements but due to high dissipativeness, one would expect that most of the bulk kinetic energy would be radiated away and therefore the terminal hot spot would in fact be fainter than on the side where no jet (and therefore no dissipation of kinetic energy) is seen. *The observed trend is thus consistent with the supposition that the jets and hot spots are both at least mildly relativistic.*

Of course, if the outflow were intermittent, then the jet could point to the brighter (newer) hot spot with neither the jets nor the hot spots needing to be Doppler enhanced. But then the correlation of jet detectability with R (e.g., Saikia, 1984b), or tendency of larger R quasars to have larger surface brightness ratios (Section 4.5) are not explained.

4.6 The flip-flop model

It is fairly common in the case of radio quasars, that the separation ratio shows marked departures from the symmetric value of unity. One of the hypotheses that has been advanced to explain this is that ejection of effluents from quasar nuclei occurs on only one side at a time (Rudnick & Edgar, 1984). If that is the case, the

"one-sided" quasars best exemplify such a phenomenon.

The primary motivation for advocating this "flip-flop" hypothesis was the phenomenon of "preferential avoidance" of radio structures of high surface brightness at the same angular separation from the nucleus. One way in which Rudnick & Edgar (1984) demonstrated this was by pointing out a "dip" at the value of unity in the distribution of separation ratios of quasars from their sample.

While the data presented here cannot be used to disprove the flip-flop hypothesis, Figs.4.4a to d show that none of the four samples of quasars considered here (which *do* satisfy the selection criteria of Rudnick & Edgar, 1984), show any evidence for the presence of a "Rudnick dip". Indeed, Kapahi & Saikia (1982) had pointed out that the bias in the sample of Rudnick & Edgar (1984) against objects with weak core components together with measurement errors could well be the causes of the "Rudnick dip". It may be noted that the trend for large separation ratios to occur in quasars with large values of R_{emit} does not find an explanation in the Rudnick & Edgar scenario. Nor does the trend that samples with large asymmetry in surface brightness of the outer components show systematically larger values of R_{emit}. Thus it is unlikely that one-sided ejection is a common phenomenon in quasars. However, the above statements are statistical, and individual cases to the contrary are not ruled out. A case in point is one of the objects in the D2 sample, viz., 1729+501. This is a one-sided source even with the present high dynamic range observations (Fig.3.33a, b and c, Chapter 3), and has a very weak nuclear radio component (R = 0.07). The lower limit to the ratio of surface brightness of the outer peaks of emission is very large. Therefore it does not

fit into the relativistic beaming scenario, and may well be an illustration of one-sided ejection. While examples of this type are not common, it must be pointed out that due to the fact that the radio nuclear component is weak, such sources may remain optically unidentified and therefore missed.

4.7 The excess of core components with steep spectrum

Kapahi (1981a) had found that the radio spectral indices of the central components of the quasars in his sample had a much wider distribution (0.4 to −1) than was known for "two-sided" quasars. Two possibilities had been suggested by him as causes of this difference: that the core components had "compact double" structure (known to occur in several radio galaxies) or were synchrotron self-absorbed at low frequencies, or alternatively, that these central components consisted of subcomponents of both flat and steep radio spectrum, such as a core with a jet, or a core with an outer lobe close by.

The high resolution images of chapter 3 support the latter alternative in the case of five of the total of nine sources suspected of having nuclear components of steep radio spectrum by Kapahi (1981a): 0003-003, 0919+218, 1010+123 and 1509+158. All of these objects have lobes of low surface brightness close to the nuclear components which were unresolved from the latter in the earlier observations; 1132+303 has a core and jet that are explicit in the new image. As for the remaining four quasars, in the case of 0615+578 which is a triple source, the northwestern lobe (which, of course, has a steep radio spectrum) was the component coincident with the proposed identification which has been subsequently found to be wrong. The same is probably true of 1547+309 (see Section 3.3 of this thesis). In

the case of 0740+380 and 1047+096, the new images show that what were previously regarded as the core components are actually independent quasars, and therefore their steep radio spectrum is no surprise.

4.8 The implied speeds of bulk motion

If the radiating, intrinsically symmetric twin beams of plasma are moving at relativistic speeds, then the ratio of the surface brightness of the approaching component to that of the receding one is given by

$$\left[\frac{1+\beta\cos\theta}{1-\beta\cos\theta}\right]^{2-\alpha}$$

For inclination angles $\leq 25°$, the values of β required for bulk motion to produce the observed surface brightness ratios in the D2 sample range from ~0.3 to ~0.7. These velocities are higher than what has been generally assumed or inferred for the large scale jets. They are certainly higher than the values derived from ram pressure confinement of the hot spots. However, the parameter that is deduced from the latter arguments is the speed of advance of the hot spot, and, as has been pointed by Blandford (1984) and Lind & Blandford (1986), the flow speeds of the complex shock patterns can be higher than the speeds of hot spot advancement.

4.9 Summary

The question of whether bulk relativistic motion on a scale of several hundred kiloparsecs can explain the structural asymmetry in radio quasars was explored in this chapter. It was argued that CSS quasars need to be excluded from analyses done within a simple relativistic beaming framework, because for these quasars R

may not be a good statistical measure of the angle of inclination of their jets.

It was shown that radio quasars with large side-to-side asymmetry in surface brightness tend to have more prominent radio nuclear components and smaller projected linear sizes. This is consistent with the prediction that they are inclined at small angles to the line of sight, and that the asymmetry is due to bulk relativistic motion.

Although in the simple relativistic beaming picture light-travel-time differences are expected to result in large separation ratios of the outer components for quasars oriented close to the line of sight, only a marginal effect is observed. Intrinsic misalignments and side-to-side differences in the characteristics of the interstellar medium could, however, mask the effect of light-travel-time differences.

For the quasars analyzed, the detected jet points to the brighter of the two hot spots in all but one case, implying mild relativistic velocities for not only the jets but also the hot spots. Only mild relativistic speeds are required of the hot spots to explain these results. Further, if the large scale jets and outer hot spots were as relativistic as the nuclear jets, R would not be expected to correlate with the degree of side-to-side asymmetry or jet detectability, because R is a measure of orientation *provided* there is a substantial difference in the Doppler enhancement of the nucleus as compared to the outer structure. Thus, the results presented in this chapter also suggest that extreme relativistic velocities in the outer components of quasars are ruled out.